

Morphology and Evolution of Simulated and Optical Clusters: A Comparative Analysis

Nurur Rahman¹ \star , Janusz Krywult², Patrick M. Motl³, Piotr Flin², and Sergei F. Shandarin

¹*Department of Physics and Astronomy, University of Kansas, Lawrence, KS 66045, USA;*

²*Institute of Physics, Pedagogical University, Kielce, Poland;*

³*Department of Physics and Astronomy, Louisiana State University, Baton Rouge, LA 70803, USA;*

nurur@kusmos.phys.ku.edu, krywult@pu.kielce.pl, motl@rouge.phys.lsu.edu, sfflin@cyf-kr.edu.pl, sergei@ku.edu

ABSTRACT

We have made a comparative study of morphological evolution in simulated DM halos and X-ray brightness distribution, and in optical clusters. Samples of simulated clusters include star formation with supernovae feedback, radiative cooling, and simulation in the adiabatic limit at three different redshifts, $z = 0.0, 0.10$, and 0.25 . The optical sample contains 208 ACO clusters within redshift, $z \leq 0.25$. Cluster morphology, within 0.5 and $1.0 \text{ h}^{-1} \text{ Mpc}$ from cluster center, is quantified by multiplicity and ellipticity.

We find that the distribution of the dark matter halos in the adiabatic simulation appear to be more elongated than the galaxy clusters. Radiative cooling brings halo shapes in excellent agreement with observed clusters, however, cooling along with feedback mechanism make the halos more flattened.

Our results indicate relatively stronger structural evolution and more clumpy distributions in observed clusters than in the structure of simulated clusters, and slower increase in simulated cluster shapes compared to those in the observed one.

Within $z \leq 0.1$, we notice an interesting agreement in the shapes of clusters obtained from the cooling simulations and observation. We also notice that the different samples of observed clusters differ significantly in morphological evolution with redshift. We highlight a few possibilities responsible for the discrepancy in morphological evolution of simulated and observed clusters.

Key words: clusters: morphology - clusters: evolution - clusters: structure - clusters: statistics

1 INTRODUCTION

The hierarchical clustering is the most popular model for the Large Scale Structure (LSS) formation. The model relies on the assumption that larger structures result from the merging of smaller sub-clumps. Theoretical paradigm of the hierarchical evolution is the Cold Dark Matter (CDM) scenario which assumes that baryonic matter (stars, hot X-ray gas) evolves in the dark matter (DM) potential through violent processes. Structural evolution in cosmological objects such as galaxies or clusters of galaxies is the underlying principle in this scenario. A generic prediction of the CDM model is the nonsphericity of the DM halos. The degree of flattening of the halos evolves in cosmological time, from highly irregular at the distant past towards more regular at the present.

In principle, the model prediction can be tested comparing the DM halo shapes with that of the (baryonic) matter distributions. A comparative morphological analysis between model and observation could help constraining the nature of the DM and its role on the LSS.

Melott, Chambers & Miller (2001; hereafter MCM) have reported evolution in the gross morphology of galaxy-clusters (quantified by ellipticity) for a variety of optical and X-ray samples for $z < 0.1$. They infer that the evidence is consistent with a low matter density universe. Using a similar shape measure as well as intra-cluster medium temperature and X-ray luminosity, Plionis (2002) has presented evidence for recent evolution in optical and X-ray cluster of galaxies for $z \leq 0.18$. In both studies evolution is quantified by the change of cluster ellipticity with redshift. In a recent study, Jeltema et al. (2005) have reported structural evolution of clusters with redshift where cluster morphology is quantified by the power ratio method (Buote & Tsai 1995). Jeltema et al. used a sample of 40 X-ray clusters over the

\star National Research Council (NRC) postdoctoral fellow; Current address: IPAC/California Institute of Technology, Mail Code 100-22, Pasadena, CA 91125, USA; Email: nurur@ipac.caltech.edu

redshift range $\sim 0.1 - 0.8$ obtained from Chandra Observatory. In spite of methodological differences, the results of these studies indicate evolution in the morphology of the largest gravitationally bound systems over a wide range of look-back time.

The observational evidence prompted concerns about the formation and evolution of structures in the CDM scenario via numerical simulations. If the results of simulations provide faithful representations of the evolutionary history of cosmological objects, then one would expect a similar trend in the structure of simulated objects. So far almost all studies of simulated clusters are focused either on understanding the nature of the background cosmology within which the present universe is evolving (Jing et al. 1995; Crone, Evrard & Richstone 1996; Buote & Xu 1997; Thomas et al. 1998; Valdarnini, Ghizzardi & Bonometto 1999; Suwa et al. 2003) or on understanding the distribution and shape of the DM halos in various types of simulations, e.g., simulations with or without baryons and gas physics (Dubinski & Carlberg 1991; Dubinski 1994; Aninos & Norman 1996; Tissera & Dominguez-Tenreiro 1998; Bullock 2001; Buote et al. 2002; Jung & Suto 2002; Gao et al. 2004a,b; Kazantzidis et al. 2004; Springel, White & Hernquist 2004; Allgood et al. 2005; Nagai & Kravtsov 2005; Flores et al. 2005; Libeskind et al. 2005; Maccio et al. 2005; van der Bosch et al. 2005; Zentner et al. 2005). Until recently a comparative study of morphological evolution in simulated and real clusters was absent. Floor et al. (2003) and Floor, Melott & Motl (2004; hereafter FMM) have investigated evolution in cluster morphology simulated with different initial conditions, background cosmology, and different physics (e.g. simulation with or without radiative cooling). They have used eccentricity as a probe to quantify evolution. Their studies, emphasizing shape in the outer regions of clusters, suggest slow evolution in simulated cluster shapes compared to the observed one. However, the studies of Floor and collaborators are indirect in a sense that they did not analyze observed clusters using the same measurement technique applied to their simulated data sets.

In this paper we make a comparative analysis between simulated and observed clusters where both data sets are juxtaposed and analyzed using the same set of structural measures. We analyze cluster morphology and its evolution using shape measures such as multiplicity (M) and ellipticity (ϵ) derived from the Minkowski functionals (Rahman & Shandarin 2003, 2004, hereafter RS03 and RS04; Rahman et al. 2004). The MFs provide a non-parametric description of the images with no prior assumptions made on the shapes of the images. The measurements based on the MFs appear to be robust and numerically efficient when applied to various cosmological studies, e.g., galaxies, galaxy-clusters, CMB maps etc. (Mecke, Buchert & Wagner 1994; Schmalzing et al. 1999; Beisbart 2000; Beisbart, Buchert & Wagner 2001; Beisbart, Valdarnini & Buchert 2001; Kerscher et al. 2001a, 2001b; Shandarin, Sheth & Sahni 2004). Various measures, constructed from the two-dimensional scalar, vector, and several tensor MFs have been described and tested in RS03 and RS04. To derive the parameters applied in this study we use the extended version of the numerical code developed in RS03 and RS04.

We study evolution in the simulated clusters in a flat CDM universe (Λ CDM; $\Omega_m = 0.3$, $\Omega_\Lambda = 0.7$) obtained from

three different sets of high resolution simulations (Motl et al. 2004). The first set has clusters simulated in the adiabatic limit, the second set contains clusters with radiative cooling (RC), and the last set includes clusters with cooling + star formation and supernovae feedback (SFF). Each sample contain DM as well as X-ray brightness distributions at three different redshifts, $z = 0.0, 0.1$, and 0.25 . For comparison we also analyze a sample of ACO (Abell, Corwin & Olowin 1989) clusters within $z \leq 0.25$. The sample contains 208 optical clusters derived from 10-inch photographic plates taken with the 48-inch Palomar Schmidt Telescope (Trèvese et al. 1992; Flin et al. 1995; Trèvese et al. 1997; Flin et al. 2000).

The objective of our study is twofold: first, to check the efficiency of the parameters differentiating various sets of objects, and second, to explore (statistical) correspondence in the morphological properties of the distributions of DM halos, X-ray emitting gas, and optical clusters using measures that are sensitive to shape and sub-structures.

In the CDM model (satellite) galaxies are associated with the DM sub-halos that are accreted by their (current) parent halo, a bigger structure usually associated with a galaxy cluster. If this is the case statistical properties of galaxies regarding mass, sub-structure, shape etc., would show a similar trend to that of the sub-halos. On the other hand X-ray emitting hot gas, evolving in the DM background potential, would not directly follow the DM distribution because of its isotropic pressure support. Therefore, a statistical analysis of various properties of DM halos, galaxy clusters, and X-ray gas distributions will be useful to probe possible bias of luminous galaxies toward sub-halos and their correspondence with the distribution of hot gas. This is the motivation behind the second objective.

The organization of the paper is as follows: simulation technique and the observational data are described briefly in §2, a short discussion of shape measures is given in §3. The results are presented in §4 and the conclusions are summarized in §5.

2 DATA

2.1 Numerical Simulations

We have analyzed images of simulated clusters projected along three orthogonal axes. The clusters have been simulated in the standard, flat cold DM universe (Λ CDM) with the following parameters: $\Omega_b = 0.026$, $\Omega_m = 0.3$, $\Omega_\Lambda = 0.7$, $h = 0.7$, and $\sigma_8 = 0.928$. For a complete description of the simulations see Motl et al. (2004). We have used three samples of clusters derived from the same initial conditions and background cosmology. The difference between the samples is in the energy loss mechanism experienced by the baryonic fluids. In the first sample, no energy loss is allowed; in the second sample fluid is allowed to lose energy via radiation and subsequently cool; in the third sample, physics of star formation and supernovae feedback are incorporated in addition to radiative cooling.

The simulations use a coupled N-body Eulerian hydrodynamics code (Norman & Bryan 1999; Bryan, Abel & Norman 2000) where the dark matter particles are evolved by an adaptive particle-mesh, N-body code. The PPM scheme

(Colella & Woodward 1984) is used to treat the fluid component on a comoving grid. An adaptive mesh refinement (AMR) is employed to concentrate the numerical resolution on the collapsed structures that form naturally in cosmological simulations. The DM particles exist on the coarsest three grids; each sub-grid having twice the spatial resolution in each dimension and eight times the mass resolution relative to its parent grid. At the finest level, each particle has a mass of $9 \times 10^9 h^{-1} M_{\odot}$. A second order accurate TSC interpolation is used for the adaptive particle mesh algorithm. Up to seven levels of refinement are utilized for the fluid component, yielding a peak resolution of $15.6 h^{-1}$ kpc within the simulation box with sides of length $256 h^{-1}$ Mpc at the present epoch. Clusters are selected using the HOP algorithm (Eisenstein & Hut, 1998) with an overdensity threshold of 160.

A tabulated cooling curve (Westbury & Henriksen 1992) for a plasma of fixed, 0.3 solar abundance has been used to determine the energy loss to radiation. Heat transport by conduction is neglected in the present simulations since it has been shown that even a weak, ordered magnetic field can reduce conduction by two to three orders of magnitude from the Spitzer value (Chandran & Cowley 1998). However, Narayan & Medvedev (2001) has shown that if the chaotic magnetic field fluctuations extends over a sufficiently large length scales within the intra-cluster medium (ICM), then thermal conductivity becomes significant to the global energy balance of the ICM. Energy input into the fluid from AGN is also neglected in the current simulations.

The prescription of Cen & Ostriker (1992) has been used to transform collapsing and rapidly cooling gas into collisionless star particles. At the finest resolution level, a grid cell is eligible to form a star in a given time step if the local flow is converging, the dynamical time exceeds the cooling time and a Jean's mass worth of gas exists within the cell. To model a population of prompt supernovae, thermal feedback has been introduced. The amount of feedback has been set from numerical experiments to provide a reasonable amount of mass in star particles. The feedback is approximately 7×10^{48} ergs per solar mass of stars formed or about half a keV of energy per particle in the final clusters.

We have 41 three dimensional clusters from each sample, giving a total of 123 projected clusters in the respective samples. Each projection is constructed within a $8 h^{-1}$ Mpc (comoving) frame containing 360×360 pixels. Majority of clusters in each sample is in the mass range $\sim 10^{13} - 10^{14} M_{\odot}$ with few clusters (~ 15) in the limit $\sim 10^{15} M_{\odot}$.

2.2 Optical Clusters

The details of data acquisition and processing of the optical sample has been described in Trèvese et al. 1992; Flin et al. 1995; Trèvese et al. 1997; Flin et al. 2000. Here we highlight only the essential features of the sample needed for this study.

The sample contains 208 optical clusters, within $z \leq 0.25$, derived from 10-inch photographic plates taken with the 48-inch Palomar Schmidt Telescope. It contains rich and massive ACO clusters with richness $R \geq 1$ and mass, approximately, in the range $\sim 10^{13} - 10^{14} M_{\odot}$. Highly massive structures, e.g. Coma cluster (A1654) or clusters constituting Shapley condensation, are absent in this sample.

The visual control is the greatest advantage of this sample. The essential difference between this and other samples is visual control of all objects classified as galaxies when automatic procedure were applied. The visual inspection was made for objects with magnitude range at least $m_3 + 3$ mag. The relationship between the number of objects with respect to the magnitude and the luminosity function for each separate cluster show that clusters are complete at least in the magnitude range m_3 to $m_{2.5}$. In majority of cases, it is complete till $m_3 + 3$.

3 MORPHOLOGICAL PARAMETERS

We use multiplicity (M) and ellipticity (ϵ) as quantitative measures to study evolution of observed and simulated clusters. Ellipticity is derived from the area tensor functional, a member of the hierarchical set of the MFs. This functional is given by,

$$A_{ij} = \int_K (x_i - A_i)(x_j - A_j) da, \quad (1)$$

where K is the region bounded by a given contour and A_i is the area vector functional, i.e. area centroid, expressed as follows,

$$A_i = \frac{1}{A_S} \int_K x_i da. \quad (2)$$

The symbol A_S represents the area within the contour. It is known as the scalar area functional and is given by,

$$A = \int_K da. \quad (3)$$

The area vector functional is in fact the center of mass of the region within the contour if we assume that the surface density of the (enclosed) region is constant. The tensor A_{ij} is closely related to the inertia tensor of a homogeneous region, The details of the MFs can be found in Schmalzing (1999), Beisbart (2000), and RS03.

- Multiplicity (M): This parameter is defined as,

$$M = \frac{1}{A_{max}} \sum_{i=1}^N A_i = \frac{A_S}{A_{max}}, \quad (4)$$

where A_i is area of the individual components at a given level, A_{max} is the area of the largest component at that level, N is the total number of components, and A_S is the total area at that level obtained after summing the areas of the components. Multiplicity, $M = M(A_S)$, is a measure with fractional value and gives the number of components measured at any brightness level: $M = 1$ for a single iso-intensity contour, i.e. component, and $M > 1$ for multi-contours.

It may be mentioned here that Thomas et al. (1998) have used multiplicity as a parameter for sub-structure measure in N-body simulations. They define it as a ratio of mass of sub-clumps to cluster mass. In this study it is a ratio of the areas (sizes) as defined in equation 1.

We use two variants of M to present our results: one is the average of multiplicity over all density/brightness levels,

\bar{M}_{eff} , and the other is the maximum of the multiplicity found at one of the levels, M_{max} .

- Ellipticity (ϵ): We adopt the definition of ellipticity,

$$\epsilon = 1 - b/a, \quad (5)$$

where a and b are the semi-axes of an ellipse. For our purpose the semi-axes correspond to the ‘‘auxiliary ellipse’’ constructed from the eigenvalues of the area tensor (see RS03 for detail). Note that the ‘‘auxiliary ellipse’’ is an ellipse having exactly the same area tensor.

We have used two variants of ϵ : one is sensitive to the shape of the individual cluster components present at a given level while the other is sensitive to the collective shape formed by all the components present at that level. We label these two variants of ϵ , respectively, as the effective (ϵ_{eff}) and the aggregate (ϵ_{agg}) ellipticity. Morphological properties of clusters such as shape and the nature or the degree of irregularity existing in these systems can be probed effectively with these two parameters.

At any given density/brightness level, we construct ϵ_{eff} as a weighted mean normalized by the multiplicity and area of the largest contour,

$$\epsilon_{eff} = \frac{1}{M \cdot A_{max}} \sum_{i=1}^N \epsilon_i A_i, \quad (6)$$

where ϵ_i are ellipticities of the individual components measured as stated earlier and M is the multiplicity at that level. The symbols A_i and A_{max} have similar meanings as before. This measure can be used as an effective tool to quantify shapes of large scale merger remnants.

To construct ϵ_{agg} , we take the union of all components present at a given level and form a collective region. The integrated region can be expressed as

$$R = R_1 \cup R_2 \cup \dots \cup R_N, \quad (7)$$

where R_i is the region enclosed by each contour. Subsequently we find the components of the area tensor and the ‘‘auxiliary ellipse’’ for the region R .

The behavior of ϵ_{agg} is similar to the conventional ellipticity measure based on the inertia tensor (Carter & Metcalf 1980). But the construction procedure of these two measures are different. The conventional method finds the eigenvalue of the inertia tensor for an annular region enclosing mass density or surface brightness. On the other hand, the method based on MFs finds the eigenvalues of regions enclosed by the contour(s) where the regions are assumed to be homogeneous.

We have computed ellipticities after averaging the estimates at all density/brightness levels. Our final result is, therefore, expressed as $\bar{\epsilon}_{eff}$ and $\bar{\epsilon}_{agg}$.

3.1 Toy Models

To get a better feeling of the parameters mentioned above we provide an illustrative example with toy models. We find this demonstration useful since it gives a visual expression how the number of group members forming complex structures affects the shapes (see also Paz et al. 2005).

One can think of these toy images as snap shots of different clusters (in projection) taken at one particular time. We include clusters with different types of internal structures in

Fig. 1: unimodal elliptic structure (panel 1), asymmetric and symmetric bimodal clusters (panels 2 and 3, respectively), cluster with filamentary structure (panel 4) etc. The multimodal clusters have clumps with different peak brightness. We show contour plots of toy clusters at different brightness levels where the levels are chosen arbitrarily. For all clusters the outer line represents the percolation level where the sub-structures merge with one another and form a single, large system.

Multiplicity as a function of component area (in grid units) is shown in Fig. 2 for our selected toy models. As mentioned earlier M is sensitive to the size of the sub-structures. The simplest case to see this is a bimodal cluster. For a bimodal structure with unequal sub-clumps (panel 2), the fractional value of multiplicity ($1 < M < 2$) tells us that the components of the system have different sizes. The isolated components eventually percolate giving $M = 1$ at low brightness level, i.e., at larger area. On the other hand, for a cluster with equal components $M = 2$ until percolation occurs (panel 3). For clusters with three components (panels 4 and 5), we see that for a small range of brightness levels, the components are well separated where two of these are bigger than the third one ($2 < M < 3$). Afterward two of the three clumps merge together giving $1 < M < 2$. These two remaining components eventually percolate to become a single system. The clumps in panel 6 are distributed around the center. For this cluster, we see two unequal but well separated clumps ($1 < M < 2$) with the same peak brightness. The behavior of clusters in panels 7 and 8 is similar except that they have a different number of sub-structures. The cluster in panel 9 has the largest number of components (a total of 7). Two of its clumps are so large compared to the other ones that they dominant. The multiplicity is always in the range $1 < M < 3$ reflecting the merger of clumps at different levels.

Ellipticity for these toy clusters is shown in Fig. 3. In this figure the solid and dotted line represent, respectively, ϵ_{agg} and ϵ_{eff} . For the unimodal cluster in panel 1, $\epsilon_{eff} = \epsilon_{agg}$. For the bimodal cluster in panel 2, the estimate of ϵ_{eff} is weighted more by the larger component. It is zero for the case shown in panel 2. This is also true for the cluster in panel 3. However, for a bimodal system with equal sized sub-clumps but different elongation, ϵ_{eff} will give an average elongation of the two. For systems with sub-structures the estimate of ϵ_{agg} , on the other hand, tells us about the overall shape of these systems. Due to the presence of two isolated components, the system itself appears more elongated than the shape of its sub-clumps. An important point to note that the estimate provided by ϵ_{agg} depends not only on the relative sizes of the components but also on their relative separations. This is reflected in the panels containing multi-clump clusters. For equal separation, a bimodal cluster with components similar in shape but unequal in size has lower ϵ_{agg} than that of a bimodal cluster with identical shape and size (see the region $1.8 < \log_{10} A_S < 2.2$ in panels 2 and 3 in Fig. 3). In general, as the density and brightness level decreases the clumps get bigger and appear closer to one another and ϵ_{agg} gets smaller.

Note that for a multicomponent system with filamentary structure, $\epsilon_{eff} < \epsilon_{agg}$ (panel 4). On the other hand if components are distributed around the cluster center, $\epsilon_{eff} > \epsilon_{agg}$ (panel 6). The cluster in panel 5 has the unique

property that is shown separately by clusters in panels 4 and 6. In transition at a lower brightness level, the cluster changes its filamentary shape to an extended structure where the components are distributed over a region around the center. The ϵ_{agg} profile in panel 8 shows that in the range, $2.2 < \log_{10} A_S < 2.8$, the cluster develops two, almost equal size clumps that are very close to each other. The cluster in panel 7 follows the behavior of a bimodal cluster except that there is jump in between $2.6 < \log_{10} A_S < 2.8$ where the cluster changes its structure having two unequal size clumps to two equal size clumps. The shape of the cluster in panel 9 changes consistently following the merger of its clumps at different brightness levels.

In Figs. 2 and 3 we also show the variants of the parameters used later in this study. We use circle and star to represent the structural parameters, \bar{M}_{eff} and M_{max} . The respective symbols are also used for the shape parameters $\bar{\epsilon}_{eff}$ and $\bar{\epsilon}_{agg}$. Comparing this set of parameters with more general M and ϵ one can easily see how these measures response to the alignment of sub-structures and their spatial locations (filamentary, extended etc.).

3.2 Example of Simulated Clusters

We demonstrate the behaviors of M and the variants of ϵ as a function of area for a collection of simulated clusters in Figs. 4 and 5. For each sample we choose two clusters at each redshift. We use dark, gray, and faint solid lines to represent respectively, the adiabatic, RC, and SFF samples. The DM halos and X-ray clusters are shown on the left and right panels, respectively.

Figure 4 shows that both matter and X-ray clusters with cooling, generally, have a higher number of sub-clumps than those without cooling. Figure 5 shows that in most cases the central part of cluster consists of a single peak ($\epsilon_{eff} = \epsilon_{agg}$). The central region of these clusters do not appear spherical, rather this region has some degree of flattening. We see that multi-peak systems, mostly bimodal clusters with un-equal size sub-clumps ($\epsilon_{eff} < \epsilon_{agg}$), are common for these clusters. At low brightness levels, i.e. in the outer regions of clusters, the sub-clumps appear in various shapes. In some cases they merge forming one system ($\epsilon_{eff} = \epsilon_{agg}$), in few cases they appear homogeneously distributed ($\epsilon_{eff} > \epsilon_{agg}$), and in few cases they form filamentary structure ($\epsilon_{eff} < \epsilon_{agg}$). The degree of inhomogeneity ($\epsilon_{eff} \neq \epsilon_{agg}$), generally, is higher for X-ray clusters. There is a weak trend that cluster centers are more flattened than the outer parts, irrespective of the nature of simulation.

4 RESULTS

One of the objectives of this paper is to study morphological evolution in simulated and optical clusters using M (equation 4) and ϵ (equations 5 - 7) as quantitative measures. These parameters represent the shape characteristics of a set of iso-density/intensity contours corresponding to a set of density/brightness levels. The levels represent equal interval in area, i.e. size in log space, which allow higher resolution and hence higher weight to the dense, central region.

In this study, we emphasize the morphological properties of the dense, central region of clusters. We analyze

each cluster at two different threshold levels corresponding to radii $\sim 0.5 \text{ h}^{-1} \text{ Mpc}$ and $\sim 1 \text{ h}^{-1} \text{ Mpc}$ where the outer radius is within ~ 3 times the core radius (Bahcall 1999). For each radius, measurements are relative to the center.

Cluster images are smoothed by a Gaussian filter with a smoothing scale (ss) $\sim 50 \text{ h}^{-1} \text{ kpc}$. We choose this scale after trials with different values. Our experience shows that for a scale smaller than $\sim 50 \text{ h}^{-1} \text{ kpc}$, images contain too much noise whereas for a larger scale they become over smoothed. We note that smoothing affects the gross morphology without much distortion in the evolutionary trend of the parameters. The trend holds for both simulated and observed cluster samples.

In Figs. 6 and 7, we show detail properties of adiabatic and observed clusters using \bar{M}_{eff} and $\bar{\epsilon}_{agg}$. These figures show results for ss = $50 \text{ h}^{-1} \text{ kpc}$ within a radius of $0.5 \text{ h}^{-1} \text{ Mpc}$ (panels numbered 1) and $1 \text{ h}^{-1} \text{ Mpc}$ (panels numbered 2). Simulated clusters are shown by (faint) horizontal lines at three different redshifts and the optical clusters are shown by (dark) crosses. The expressions at each panel represent the best fit line relating the mean of the parameter to the redshift although we note that at each redshift the distribution functions are highly non-Gaussian. An interesting feature of these figures is that, at least within $z \leq 0.25$, optical clusters have similar dispersion in both \bar{M}_{eff} and $\bar{\epsilon}_{agg}$. Similar behavior is also noticed for other parameters in this redshift range, irrespective of simulation types. The wide spread in multiplicity and projected shape of DM halos and X-ray gas is a clear reflection of different merging history (Jing & Suto 2002). Note that the error bar in the normalizations (i.e., intercepts) of the best fit lines is less than 10% for all parameters (not shown in these figures).

We quantify the rate of evolution by the slope of the best fit line where the rate means either dM/dz or $d\epsilon/dz$. For gross morphology, we refer to the normalization of this line. We present our final results in Figs. 8 to 13 within $\sim 0.5 \text{ h}^{-1} \text{ Mpc}$ and $\sim 1 \text{ h}^{-1} \text{ Mpc}$ radii with ss $\sim 50 \text{ h}^{-1} \text{ kpc}$ both for simulated and optical samples. For simulations we show the best fit line along with its expression in gray color. We divide the optical sample into four bins with equal number of clusters in each bin. In this case the best fit line is shown in dark color. No expression is given for this line. In both simulated and observed clusters the error bar represents the error in the mean.

4.1 Comparison among Simulated Cluster Samples

A visual examination of Figs. 8 - 13 clearly shows an evolutionary trend in cluster morphology since the gross properties of clusters indeed change with redshifts. We are interested to determine the significance of this trend of cluster properties computed at two different different regions surrounding the cluster center and than to compare it with observations.

Cluster properties within $\sim 0.5 \text{ h}^{-1} \text{ Mpc}$ of the different samples are shown in Figs. 8 - 10. In terms of multiplicity, a parameter that probes the number of sub-components present in a complex system, we find that cooling samples have slightly higher value of multiplicity at all redshifts compared to that in the adiabatic sample. The low abundance of single component systems with radiative cooling indicates

that the dense, cool core sub-structures are long lived features (Motl et al. 2004). We find that the feedback mechanism with cooling makes cosmological systems less clumpy than systems without feedback. Energy feedback process, most likely, slows down the rate of evolution in the X-ray clusters than those in the cooling only samples. However, this is quite opposite for the DM halos. Higher multiplicity in the X-ray clusters in the cooling samples indicates a possibility of less efficient merging in hot baryonic gas.

In all simulations multiplicity shows a clear trend with redshift: clusters have higher (mean) multiplicity at higher redshifts. Cluster multiplicity reflects sub-structures merger rate. It decays by the rate at which the cluster can relax, a time scale which is roughly equal to the dynamical time. The CDM halos host a larger amount of substructure at higher redshifts because of lower accretion time as compared to the dynamical time (see Zentner et al. 2005). This is the reason for the systematic increase in overall sub-structures with increasing redshifts.

In terms of ellipticity, we find that the X-ray clusters, in general, are more regular than the halos. The X-ray emitting hot gas is supported by the thermal pressure. Due to its isotropic pressure support the X-ray gas becomes homogeneously distributed in the background DM potential where it evolves. As a result, morphology of the distribution of X-ray gas appears more regular. Our results suggest that in X-ray clusters the irregular sub-components are distributed over a region instead of making a filamentary structure along one direction. A comparison of $\bar{\epsilon}_{eff}$ with $\bar{\epsilon}_{agg}$ for the halos (in all samples) shows that the halo sub-clumps are not distributed uniformly around the central region. Rather these clumps are spread out mostly in one direction forming filamentary structure, as indicated by the larger value of $\bar{\epsilon}_{agg}$.

No significant evolution is signaled by $\bar{\epsilon}_{eff}$ for the DM clusters in any of these samples. Recall that this parameter is an indicator of shapes of individual components in a cluster. Therefore, no evolution means that shapes of isolated components in clusters at one redshift appear similar any other redshifts. Since it places emphasis on individual component, therefore, it is not unusual to find no evolution quantified by this parameter. However, shapes of sub-clumps in the distributions of X-ray gas change in the cooling simulations compared to other simulations.

Properties of simulated clusters within $\sim 1 \text{ h}^{-1} \text{ Mpc}$ are shown in Figs. 11 - 13. We notice that in this distance, small scale structures of simulated clusters do not change significantly than what we find in smaller scale. This implies that the small sub-clumps can exist up to a Mpc scale and distributed widely over the cluster body. However, in this scale sub-structures evolves a bit faster. We find that individual, isolated components become a bit more flattened and their evolution is slightly stronger. The overall shape of the clusters, however, is less flattened than the central region and evolution is weak in all simulations.

We take projections along each axis at a time and repeat our analysis. Recall that in this case, each sub-sample (along each axis) has only 41 clusters. The analysis of these sub-samples do not show significant variation from the primary sample. Therefore, it is unlikely that the overall result may have contaminated by the projection effect. We have also repeated our analysis using different values for the den-

sity/brightness levels. Apart from a minor change in gross morphology, we find similar results for the rate of evolution.

We summarize our main results as follows: First, the DM halos show very similar evolution in all samples of clusters. Second, the X-ray clusters in the adiabatic simulation evolve faster than those with radiative cooling. Third, morphology of the central parts of clusters evolve slightly strongly than the outer regions. Fourth, feedback processes with cooling makes the DM halos slightly more flattened and slower in evolution than the cooling only simulations (see Kazantzidis et al. 2004 for a similar trend).

We emphasize that the measured quantities for the DM distributions in all three samples are very similar. This is a check on the consistency of the simulations and analysis. The result is expected as the N-body segment of the simulations are identical in all three cluster samples with the exception of the gas that makes a relatively minor contribution to the total gravitational potential. The LSS of adiabatic and cooling clusters are generally similar but their small scale structures are determined by the overall cluster properties rather than perturbative interactions (Motl et al. 2004). In the adiabatic clusters, the mixing of in-falling sub-clumps into the main cluster medium is quicker relative to the radiative cooling clusters where sub-structures can be long lived. This is a reason behind the fast evolution of adiabatic X-ray clusters. The relaxation time scale for collisionless particles is much longer than that of the collisional gas particles (Frenk et al. 1999; Valdarnini, Ghizzardi & Bomometto 1999). Therefore, the DM halos will appear not only more elongated than the distributions of X-ray gas, but the redshift evolution of their shapes will also be slower. More spherical configurations for X-ray clusters is also expected from the point of view that intra cluster gas is approximately in hydrostatic equilibrium and supported by isotropic pressure (Sarazin 1988). The DM, on the other hand, appears to be distributed like galaxies as indicated by recent observations from gravitational lensing (Fischer et al. 1997; Fischer & Tayson 1997; Kochanek 2001; Hoekstra 2003; Hoekstra et al. 2004) and by high resolution hydrodynamical simulations (Nagai & Kravtsov 2004; Kang et al. 2005; Maccio et al. 2005).

There is a consensus based on the observations of X-ray clusters that cooling affects the mass distribution appreciably only in the inner $\sim 10\%$ of the virial radius of cluster size halos (Sarazin 1986). Contrary to that recent high resolution hydrodynamic simulations show something quite interesting (see Kazantzidis et al. 2004). Kazantzidis et al. show that there is a significant difference in overall shape between dissipationless and dissipative simulations which is persistent up to the virial radius. The virial mass of their DM halos ranges from $\approx 10^{13}$ to $3 \times 10^{14} \text{ h}^{-1} M_{\odot}$ which translates to the virial radius range $\sim 0.26 - 0.82 \text{ h}^{-1} \text{ Mpc}$ assuming $\Delta_{vir}(z=0) \sim 337$, $h \sim 0.7$, and $\rho_c \sim 1.87h^2 \times 10^{-29} \text{ gm cm}^{-3}$ (Kolb & Turner 1990; Zentner et al. 2005). Kazantzidis et al. present their analysis upto the virial radius. However, from the trend seen right at the virial radius, it seems likely that it goes a bit further down along the radial direction before shapes in dissipative and dissipational simulations converge.

Baryon fraction ($\Omega_b \sim 0.043$) in Kazantzidis et al. simulations is larger than what has been used in our simulations. Therefore, question can be raised whether low baryon den-

sity can also produce systematic shift in the shapes of DM halos to be robust on scales of Mpc as noted in our work. Our simulations use baryon density ($\Omega_b = 0.026$) and normalization of fluctuation spectrum ($\sigma_8 = 0.928$) which are slightly off than the corresponding WMAP values ($\Omega_b = 0.044$ and $\sigma_8 = 0.84$, Spergel et al. 2003). Baryon density is an important cosmological parameter which affects radiative cooling and X-ray luminosity at the central region of large virialized structures. Higher Ω_b enhances the cooling rate, subsequently making the central region more regular (Sarazin 1986, Kazantzidis et al. 2004, Springel & White 2004, Allgood et al. 2005, Flores et al. 2005). Recent numerical simulations show that larger σ_8 produces DM halos that are more regular in the central regions (Allgood et al. 2005). Therefore, we note that cooling is under-emphasized while the core DM sub-structure is over-emphasized in our simulations. It may be likely that the offset of Ω_b and σ_8 compared to WMAP would balance each other and our results obtained from the cooling simulations would still be representative had we been using the WMAP values.

With cooling only, our simulated clusters of galaxies show a large amount of long-lived substructure compared to the other simulated samples. While the amount of cooling in this sample is unphysical it represents an interesting, theoretical, limiting case. On the scale of the cluster itself, the gravitational and dynamical effects of cool, dense cores of gas have significantly altered the shape of the clusters to length scales comparable to the virial radius (see Figs. 4 & 5). The perturbation from cool baryonic clumps may thus significantly alter model dependent mass maps derived from weak lensing studies. The robust substructures present in the cooling only sample may also play a role in steepening the total cluster mass profile (Maccio et al. 2005) and with higher resolution simulations may bound the possible contribution of substructures to strong lensing in clusters. Though beyond the scope of the current paper, these connections to lensing studies will be pursued in future work.

Numerical simulations provide interesting information on two different aspects of the LSS: 1) shape of the central structures in galaxy or cluster size halos, and 2) Change in shape of halos with radial distance, irrespective of the nature of simulation. Recent high resolution hydrodynamical simulations has shown quite successfully that hydrodynamical phenomena make cluster centers considerably more spherical than those in the adiabatic simulations. However, radial dependence of shape is still a controversial issue. While Frenk et al. (1988), Bullock (2002), Springel, White & Hernquist (2004), Hopkins, Bahcall & Bode (2005), and hydro simulation of Kazantzidis et al. (2004) agree that inner part of clusters are more spherical than the outer part, the following groups of Dubinski & Carlberg (1991), Warren et al. (1992), Jung & Suto (2002), Allgood et al. (2005), and hydro simulation of Tissera & Dominguez-Tenreiro (1998) find it completely opposite. Our results closely follow the latter group.

Note that radial dependence of shape is not monotonic. It changes in a quite complicated way depending on the presence of sub-clumps as one can see from Fig. 5. A similar trend is also seen in hydro simulations of Kazantzidis et al. (2004).

4.2 Comparison with Optical Clusters

We have analyzed a sample of ACO clusters within redshift, $z \leq 0.25$. The sample contains 208 optical clusters derived from 10-inch photographic plates taken with the 48-inch Palomar Schmidt Telescope (for details of the data acquisition and processing see Trèvese et al. 1992; Flin et al. 1995; Trèvese et al. 1997; Flin et al. 2000). Results obtained from the optical clusters are shown in Figs. 8 - 13 using dark dashed lines. The summary of our results is as follows:

- The optical clusters are, in general, more clumpy than the simulated DM halos as given by both \bar{M}_{eff} and M_{max} . The sub-structure at the central part of X-ray clusters in the RC sample are compatible with the optical clusters, at least, within redshift $z \leq 0.25$. At large radius, the optical clusters include more small scale structures and show stronger evolution in sub-structures.

- The sub-structures of hot baryonic gas evolve much strongly in the adiabatic simulation than that in the galaxy distribution ($d\bar{M}_{eff}/dz \sim 0.14, 0.13$ in 0.5 and $1 \text{ h}^{-1} \text{ Mpc}$). On the other hand, effective sub-clumps (\bar{M}_{eff}) of the halos have faster rate in both adiabatic and SFF simulations. Feedback process along with radiative cooling make rapid evolution in DM halo structures. In terms of M_{max} , however, evolution of the galaxy distribution is always stronger compared to all three simulations ($dM_{max}/dz \sim 0.57, 0.79$ for 0.5 and $1 \text{ h}^{-1} \text{ Mpc}$, respectively).

- The largest component of the DM halos (probed by $\bar{\epsilon}_{eff}$) in the adiabatic and SFF simulations have higher elongation compared to that in the galaxy distribution. In the RC simulation we find an opposite trend. The shape of the largest sub-clump formed in the distributions of X-ray emitting hot gas in all three simulations are significantly rounder than that of the optical clusters ($d\bar{\epsilon}_{eff}/dz \sim 0.27, 0.22$ in 0.5 and $1 \text{ h}^{-1} \text{ Mpc}$, respectively).

- The overall shape (probed by $\bar{\epsilon}_{agg}$) and the strength of evolution in optical clusters ($d\bar{\epsilon}_{agg}/dz \sim 0.28, 0.2$ in 0.5 and $1 \text{ h}^{-1} \text{ Mpc}$, respectively) show nice agreement with that of the X-ray clusters in dissipative simulations. In dissipationless simulation, however, hot gas is systematically less elongated but evolve much strongly than the galaxy distribution ($d\bar{\epsilon}_{agg}/dz \sim 0.28, 0.2$ in 0.5 and $1 \text{ h}^{-1} \text{ Mpc}$, respectively).

- The shapes of the optical clusters are comparable to the halos only in the RC simulation. The halos are slightly more flattened and slower in evolutionary process compared to the galaxy distributions in the adiabatic case and in simulation including feedback processes with cooling.

- The strength of shape evolution given by $d\bar{\epsilon}_{agg}/dz$ is slightly stronger around the cluster core, in both observed and simulated clusters.

There are several possibilities for optical clusters to be more clumpy. First, the choice of smoothing may not be optimal for the optical sample. The smoothing scale used in our study, therefore, should be taken as the lower limit. Second, projection effect due to the background galaxies may also play an important role. This effect becomes significant as one moves away from the clusters center (Kolokotronis et al. 2001). Third, since ACO clusters are selected via richness criteria and it has been shown that richness is poorly correlated with mass (Girardi et al. 1998; Miller 2004, private communication), there is a chance that optical sample may be biased toward high mass end of cluster mass range or clus-

ters that have gone through recent merger. Massive clusters are dynamically less relaxed and hence rich in sub-structure. A well defined mass selection criteria needs to be applied for a more systematic comparison as recent numerical simulations show that cluster shapes depend on mass, although the mass - shape correlation is weak and show large dispersion (Bullock 2002; Jing & Suto 2002; Hopkins, Bahcall & Bode 2005; Allgood et al. 2005).

Regarding the comparison of the strength of evolution we note that the morphological parameters derived for the set of simulated halos have uniform statistical weight at all redshifts. However, this is certainly not the case for the observed sample as it has considerably more weight toward $z = 0.0$ than the simulated samples (see Figs 6 and 7). As mentioned earlier the scatter is comparable in both samples and, therefore, we believe the choice of binning has less effect on the overall outcome of our analysis.

4.3 Results from Previous Studies on Observed Clusters

In this section we summarize the results obtained from previous studies on optical and X-ray clusters. Our objective is to highlight the fact that different samples of clusters give different rates of evolution in cluster morphology. Due to the methodological differences, we refrain from making a direct comparison with the results of these studies.

To find cluster shapes, all previous studies follow the procedure described in Carter & Metcalf (1980). These studies, however, differ in adopting weighting factor, threshold level, cluster center and smoothing techniques to construct galaxy density distribution from spatial distribution. It is also important to note that cluster shape quantified by ellipticity is not uniquely defined. Therefore, to help reader getting a better feelings about the inherent differences of previous studies we also provide a brief outline of the methodologies used in these studies.

The optical sample of MCM contains 138 ACO clusters with $z < 0.1$ which has been compiled from West & Bothun (1990); Rhee, van Haarlem & Katgert (1991) and Kolokotronis et al. (2001). This sample show no significant evolution, $d\epsilon/dz \sim 0.03$.

The former two groups measure cluster shapes from discrete galaxy distribution using method of moments. They define the two-dimensional moments as,

$$\mu_{mn} = \frac{\sum_{i,j} (x_i - x_0)^m (y_j - y_0)^n}{N}, \quad (8)$$

where x_0, y_0 are the coordinates of the brightest galaxy taken as the cluster center, N is total number of galaxies within the region which is 3σ above the background noise and $m, n = 0, 1, 2$. They diagonalize the matrix formed by the components μ_{20}, μ_{02} , and μ_{11} , find the eigenvalues and obtain cluster shape using eigenvalues from the relation, $\epsilon = 1 - \lambda_2^2/\lambda_1^2$, where $\lambda_1 > \lambda_2$. Kolokotronis et al. (2001) use moment of inertia method for a sample containing 22 APM clusters along with their ROSAT counterparts in the redshift range, $z \leq 0.13$. They use Gaussian smoothing on galaxy density distribution and define the components of the

symmetric inertia tensor as,

$$I_{11} = \sum_i w_i (r_i^2 - x_i^2), \quad I_{22} = \sum_i w_i (r_i^2 - y_i^2), \\ I_{12} = I_{21} = - \sum_i w_i x_i y_i, \quad (9)$$

where w_i is the average cell density within $0.75 \text{ h}^{-1} \text{ Mpc}$ region and $r_i^2 = x_i^2 + y_i^2$. After defining inertia tensor, Kolokotronis et al. follow similar route to the other groups to define shape except that they define ellipticity as, $\epsilon = 1 - \lambda_2/\lambda_1$.

Plionis (2002) analyze the largest sample of optical clusters following the method used in Kolokotronis et al. (2001). His sample has 407 APM clusters within a volume of $z < 0.18$. The rate of evolution for the Plionis sample is $d\epsilon/dz \sim 0.7$. However, if both are combined, replacing the common ones by the APM clusters, the rate increases. The combined sample of ~ 500 optical clusters with $z < 0.18$ shows $d\epsilon/dz \sim 1.06$.

It is rare to find a large sample of X-ray clusters with up-to-date ellipticity measurements. The X-ray sample of MCM is compiled from Mcmillan, Kowalski & Ulmer (1989; hereafter MKU) and Kolokotronis et al. (2001). MKU measure cluster shape using method of moments from 2D X-ray surface brightness images. They adopt the following definition of the moment,

$$\mu_{mn} = \frac{\sum_{i,j} f_{ij} (x_i - x_0)^m (y_j - y_0)^n}{\sum_{i,j} f_{ij}}. \quad (10)$$

where x_0, y_0 are the components of the image centroid, $x_0 = \sum x_i f_{ij} / \sum f_{ij}$ and $y_0 = \sum y_j f_{ij} / \sum f_{ij}$. They determine the overall shape of a cluster using the faintest flux level available for that object. This sample has 48 clusters with $z < 0.1$ which is three times smaller than the MCM optical sample and an order of magnitude smaller than the APM sample. It also has a lower redshift limit than the APM sample. The rate of evolution for this sample is $d\epsilon/dz \sim 1.7$. The result suggests faster evolution for the X-ray clusters than the optical one. Interestingly, a comparison of optical and X-ray clusters within Kolokotronis et al. (2001) sample show completely opposite trend: galaxy density distributions have stronger evolution than the distribution of hot gas. The galaxy and X-ray cluster shapes follow a trend where flattened gas distribution signals anisotropic distribution of galaxies. However, the scatter is large in both relationships. It is not clear to us what could be the reasons of possible contradictions except the fact that MCM sample is most likely contaminated due to different methodologies. Besides it is also difficult to make any definite conclusion because of the smaller sizes of the samples. A large sample of X-ray clusters with better selection criteria and extended to higher redshift is needed.

We reanalyze $\epsilon - z$ estimates derived from the APM cluster data and the combined sample imposing a redshift cutoff $z < 0.1$ in order to be consistent with the redshift range of MCM X-ray sample. For these samples, we find the rate of evolution as, $d\epsilon/dz \sim 1.02$ and ~ 1.0 , respectively. We find that evolution of optical clusters accelerates in this redshift range but it is still slower than that of the X-ray.

Flin, Krywult & Biernacka (2004; hereafter FKB) has analyzed a sample of 246 ACO clusters for $z \leq 0.31$. This

group use the same definition of moment as in equation 1. They use density peak as the cluster center and measure shapes at different circular aperture radii ranging from 0.5 to 1.5 h^{-1} Mpc with an increment of 0.25 h^{-1} Mpc. They estimate cluster shape at all radii and find no dependence of cluster ellipticity on redshift. Interestingly FKB noted a decrement of $d\epsilon/dz$ with radius. They find positive evolution at radii of 0.5 and 0.75 h^{-1} Mpc. However, for radii ≥ 1 h^{-1} Mpc, they report negative evolution. The mean of their estimates derived from these five radii shows $\bar{\epsilon} \approx 0.22$ and $d\bar{\epsilon}/dz \sim 0.013$. For $z < 0.1$, their result also indicates weak evolution. We use this sample of optical clusters for our analysis (see §4.2) but with a reduced number (208) of clusters. The reduction is made after visual inspection and it is due to the removal of clusters images that appear either small or close to the boundary.

It should be noted that MCM and APM samples emphasize cluster morphology in two different regions. The MCM sample excludes any study with radius less than 1 h^{-1} Mpc and includes the estimate of ellipticity within $\sim 1 - 2$ h^{-1} Mpc from the cluster center. The APM sample, however, provide information on cluster shape within 0.75 h^{-1} Mpc of the center. Therefore, care must be exercised in interpreting and comparing results of observed clusters with simulations if both are not analyzed under the same measurement technique. Unfortunately the studies of Floor et al. (2003) and FMM (2004) has ignored this fact.

In spite of differences in the evolution of cluster morphology, optical samples are consistent with one another atleast in one case: shape of galaxy density distributions evolve strongly in the central region (Plionis, 2002) than that in the outer part (MCM, 2001). Interestingly our results are also consistent with this trend. For X-ray clusters this trend has yet to establish.

5 CONCLUSIONS

Numerical simulations provide an unique opportunity to follow the hierarchical nature of the LSS formation in both linear and nonlinear regimes (Frenk et al. 1985, 1988; Quinn, Salmon & Zurek 1986; Efstathiou et al. 1988). In order to be representative of the reality, results from simulations should agree with observations. Observations provide evidence of morphological evolution in galaxy-clusters (Melott, Chambers & Miller 2001; Plionis 2002; Jeltema et al. 2005), simulations should show similar trend. Besides, in the CDM model luminous galaxies are associated with the DM sub-halos which reside in bigger parent halos, closely associated with galaxy clusters. According to this model statistical properties of galaxies, e.g. mass, sub-structure, shape etc., would show a similar trend to that of the sub-halos while X-ray emitting hot gas would have different properties than galaxies and sub-halos. A statistical analysis of various properties of halos, galaxy clusters, and X-ray gas could provide clues to find possible biasing of luminous galaxies toward DM sub-halos and whether or not they have any correspondence with the distribution of hot gas. With this in mind, we have studied redshift evolution of cluster morphology simulated, respectively, in the adiabatic limit, with radiative cooling, and with star formation including SN feedback at three different redshifts, $z = 0.0, 0.10$, and 0.25. For com-

parison we have also studied a sample of observed clusters containing 208 ACO clusters within redshift, $z \leq 0.25$.

Since observed clusters are projected along the line of sight and lack the full three dimensional information we, therefore, use projected simulated clusters. Each cluster image is a 8 h^{-1} Mpc frame containing 360×360 pixels. Clusters are analyzed at two different density/brightness threshold levels corresponding to radii 0.5 and 1 h^{-1} Mpc from the cluster center. To quantify morphological evolution we use multiplicity and ellipticity as two different probes that are sensitive to cluster sub-structures and shape.

Our results indicate that optical clusters have, in general, more sub-structures than simulated halos and X-ray brightness distributions. Cluster components, in both observed and simulated clusters, evolve with redshifts and the evolution is different at different regions from cluster centers. In terms of total multiplicity (M_{max}), observed clusters have stronger evolution compared to DM halos. The X-ray brightness distributions, however, show steeper evolution (than that of galaxy clusters) in dissipationless simulation.

We find that in terms of overall shape, simulations do model the observed universe in an interesting way. The simulated clusters evolve with redshift, consistent with the hierarchical formation scenario. However, observed clusters appear to be slightly more flattened at higher redshift than the simulated one indicating slower evolution in simulated objects. This may reflect some form of incompleteness in our understanding in simulating the LSS. Our results differ from those of FMM (2004) who reported that the evolution in the simulated cluster shape is significantly slower than the observed one. We not only find stronger structural evolution in simulated clusters, but also find that observed cluster shapes appear to be consistent with dissipative simulations, at least, in the redshift range $z < 0.1$. The discrepancies noted in FMM is due to the different redshift ranged probed as well as intrinsic methodological differences while comparing simulations with observations.

We note that on one hand shapes of optical clusters seems to be compatible with both the halos and X-ray brightness distributions, one the other hand, both of these components appear to be less clumpy than the distribution of galaxies. Therefore, it seems puzzling whether or not there is any correspondence between the DM halos and galaxies. The existence of any such correspondence is still a matter of ongoing debate as there are conflicting results based on systematics of numerical simulations such as nature of simulations (dissipationless or dissipative) and the effect of mass and force resolution (see Maccio et al. 2005). In the context of the CDM model we would expect that the optical clusters would have similar morphology and evolutionary trend to that of the halos and would be different than the properties of the distribution of hot gas traced in the X-ray region of the spectrum.

Within the uncertainties and systematics involved in our optical sample, the results indicate that the properties of optical clusters do not exactly represent either the distribution of the halos or that of the X-ray emitting gas in any of the simulations. We find offsets in the measured parameters, such as multiplicities and ellipticities, between observations and simulations, and are unable to find any clear signature of DM-galaxy biasing based on our morphological analysis. This may be an indication, although in no way conclusive,

of the fact that these components of the LSS may represent intrinsically different populations, and galaxies may not trace the DM distributions (see Gao et al. 2004a,b; Nagai & Kravtsov 2005). However, this is merely a speculation and we stress that care must be exercised in interpreting our results as one must be careful in selecting proper measures, radius, mass range, and most importantly, well defined samples of clusters to have unbiased and meaningful results in any morphological analysis comparing observations and simulations.

We find that the measurements from different samples do not agree on the evolution rate. Take, for example, optical clusters with $z < 0.1$, and radius, $0.75 h^{-1}$ Mpc. In this case, the APM sample shows $d\epsilon/dz \sim 1.02$. FKB, on the other hand, finds much weaker evolution, $d\epsilon/dz \sim 0.2$. As mentioned in FKM, the discrepancy may be due to differences in adopting cluster centers, smoothing, and applied method of shape determination.

A preliminary analysis of a sample of 800 clusters constructed from the Sloan Digital Sky Survey (SDSS) shows that ellipticity evolution of optical clusters, for $z < 0.1$ and within $\sim 1 h^{-1}$ Mpc, is weaker than that of the APM clusters. The result indicates that clusters with different mass limits evolves differently. Large, massive clusters ($M \sim 10^{15} M_{\odot}$) have stronger evolution compared to the less massive clusters ($M \sim 10^{13} - 10^{14} M_{\odot}$) (C. Miller 2004, private communication). This is an interesting observation. If it is confirmed then the scaling relation between axes ratios and mass noted in simulations (Bullock 2002; Jing & Suto 2002) must be modified to be consistent with observations.

The SDSS sample is uniform with a well documented selection function and high degree of completeness. We may then infer that the cluster samples discussed previously have less uniformity in mass range: the APM catalog and FKB samples are biased toward massive clusters whereas the MCM samples contain more less massive clusters. The discrepancy may also arise from the techniques applied in ellipticity estimates (see also Flores et al. 2005 in this regard). Unfortunately we are unable to check the evolution strength - mass relation for our optical sample because, apart from an approximate range, no well defined criteria has been used to sort clusters into different mass bins.

The discrepancy in the optical samples is an indication of different selection criteria used to construct the catalogs. Larger and more complete catalogs obtained from the SDSS and XMM-Newton survey may be able to shed more light into this issue. It is also likely that numerical simulations may lack crucial physics that needs to be included (see FMM for discussion). In the future we will analyze clusters simulated with various gas physics, e.g. thermal conduction and AGN heating, and compare them with the SDSS clusters. The results of these studies may give us some clues to gain better insight of the current discrepancy.

Acknowledgments We thank the anonymous referee for constructive comments and criticisms which help to improve the quality of this paper. We thank M. Plionis for providing the APM cluster ellipticity data and Scott W. Chambers for the MCM data sets. NR thanks Hume Feldman and Bruce Twarog for many useful discussions.

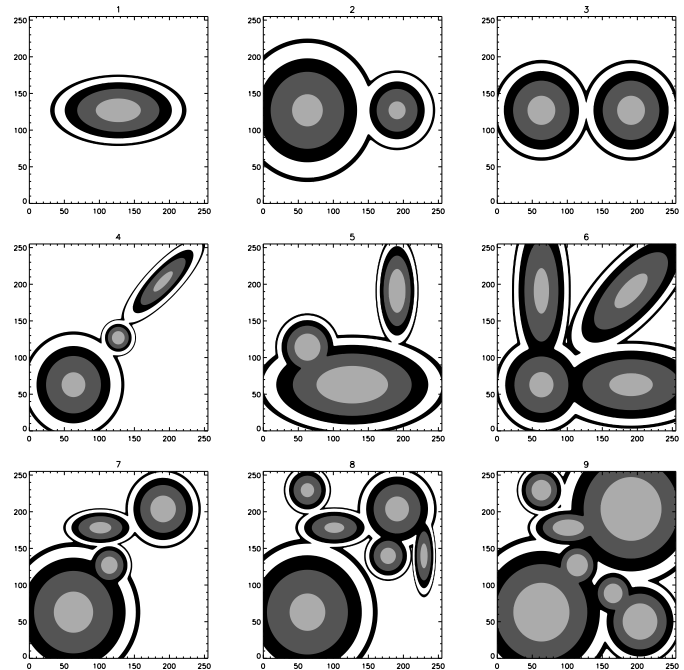


Figure 1. Contour plots of toy clusters at different brightness levels (in arbitrary scales). The multi-modal clusters have clumps with different peak brightness. For all clusters the outer line represents the percolation level where the sub-structures merge and form a single, large system.

REFERENCES

- Abell G. O., Crowin H. G., Olowin H. G., 1989, *ApJS*, 70, 1 (ACO)
- Allgood et al., 2005, *MNRAS*, submitted, astro-ph/0508497
- Aninos P., Norman M. L., 1996, *ApJ*, 459, 12
- Bahcall N. A., 1999, in *Formation of Structure in the Universe*, eds. A. Dekel & J. P. Ostriker (Cambridge University Press, New York), p. 135
- Beisbart C., 2000, Ph.D. Thesis, Ludwig Maximilians Universität, München, Germany
- Beisbart C., Buchert T., Wagner H., 2001, *Physica A*, 293, 592B
- Beisbart C., Valdarnini R., Buchert T., 2001, *A&A*, 379, 412
- Bryan G. L., Abel T., Norman M. L., 2001, *Proceedings of Supercomputing*, <http://www.sc2001.org/>
- Bullock J. S., 2002, in *The Shapes of Galaxies and Their Dark Matter Halos*, ed. Priyamvada Natrajan (World Scientific, Singapore), p. 109, astro-ph/0106380
- Buote D. A., Tsai J. C., 1995, *ApJ*, 452, 522
- Buote D. A., Xu G., 1996, *MNRAS*, 284, 439
- Buote D. A., Jeltema T. E., Canizares C. R., Garmire G. P., 2002, *ApJ*, 577, 183
- Carter D., Metcalfe N., 1980, *MNRAS*, 191, 325
- Cen R. & Ostriker J. P., 1992, *ApJ*, 393, 32
- Chandran B. D. G., Cowley S. C., 1998, *Phys. Rev. Lett.* 80, 3077
- Colella P., Woodward P. R., 1984, *J. Comput. Phys.*, 54, 174
- Crone M. M., Evrard A. E., Richstone D. O., 1996, *ApJ*, 467, 489
- Dubinski J., Carlberg R. G., 1991, *ApJ*, 378, 496
- Dubinski J., 1994, *ApJ*, 431, 617
- Efstathiou G. P., Frenk C. S., White S. D. M., Davis M., 1988, *MNRAS*, 325, 715
- Eisenstein D. J., Hut P., 1998, *ApJ*, 498, 137
- Fischer P., Bernstein G., Rhee G., Tyson J. A., 1997, *AJ*, 113, 521
- Fischer P., Tyson J. A., 1997, *AJ*, 114, 4

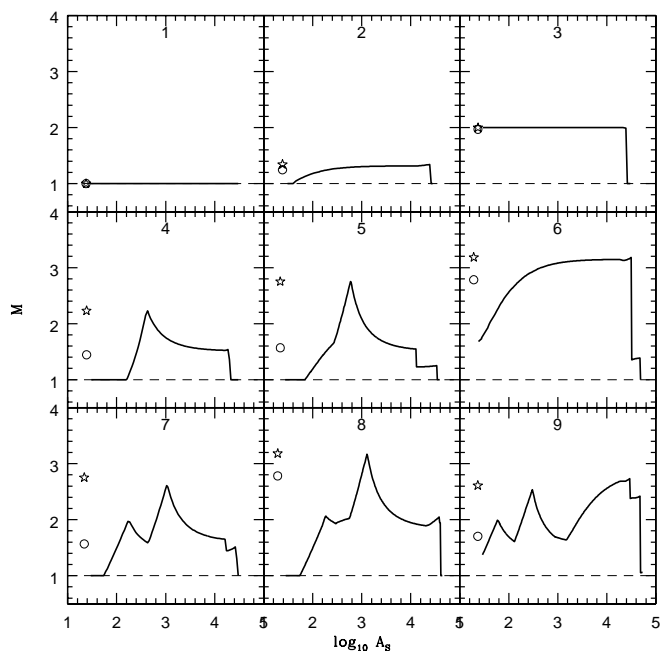


Figure 2. Multiplicity as a function of contour area (A_S) for toy clusters as shown in Fig. 1. The circle (star) represents the effective multiplicity \bar{M}_{eff} (maximum multiplicity M_{max}) as defined in the text. The x-coordinates of these legends are chosen only for the convenience of demonstration. Recall that the position of the highest peak along the x-axis corresponds to the M_{max} whereas \bar{M}_{eff} is obtained after averaging along the x-axis. See text for details.

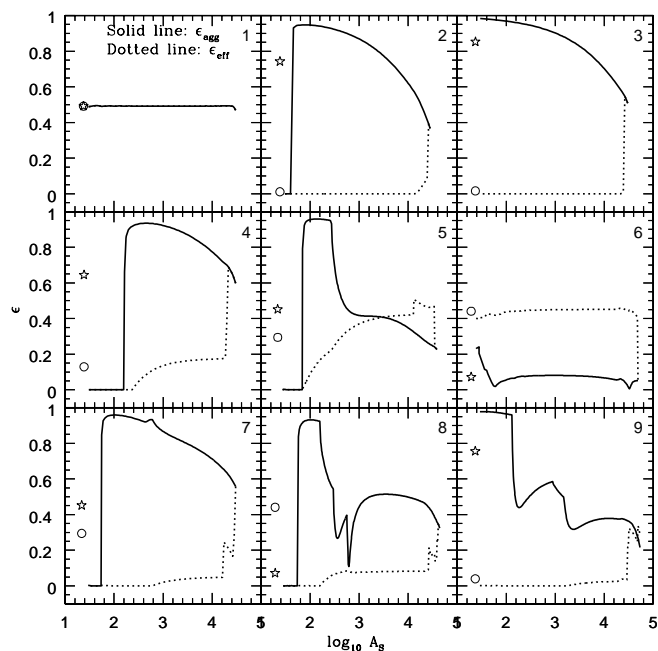


Figure 3. Ellipticity as a function of contour area (A_S) for toy models as shown in Fig. 1. Dotted and solid lines represent, respectively, ϵ_{eff} and ϵ_{agg} . The circle (star) represents the $\bar{\epsilon}_{eff}$ ($\bar{\epsilon}_{agg}$) for these toy clusters as defined in the text. Once again the x-coordinates of these legends are chosen only for the convenience of demonstration. See text for details.

Flin P., Trèvese D., Cirimele G., Hickson P., 1995, *A&AS*, 110, 313
 Flin P., Krywult J., Trèvese D., Cirimele G., Hickson P., *A&ASS*, 146, 373
 Flin P., Krywult J., Biernacka M., 2004, astro-ph/0404182 (FKB)
 Flores R. A., Allgood B., Kravtsov A. V., Primack J. R., Buote D. A., Bullock J. S., *MNRAS*, submitted, astro-ph/0508226
 Floor S. N., Melott A. L., Miller C. J., Bryan G. L., 2003, *ApJ*, 591, 741
 Floor S. N., Melott A. L., Motl P. M., 2004, *ApJ*, 611, 153 (FMM)
 Frenk C. S., White S. D. M., Efstathiou G. P., Davis M., 1985, *Nature*, 317, 595
 Frenk C. S., White S. D. M., Davis M., Efstathiou G. P., 1988, *ApJ*, 327, 507
 Frenk C. S. et al., 1999, *ApJ*, 525, 554
 Gao L., de Lucia G., White S. D. M., Jenkins A., 2004a, *MNRAS*, 352, L1
 Gao L., White S. D. M., Jenkins A., Stoehr F., Springel V., 2004b, *MNRAS*, 355, 819
 Ghigna S., Moore B., Governato F., Lake G., Quinn T., Stadel J., 1998, *MNRAS*, 300, 146
 Girardi M., Borgani S., Giuricin G., Mardirossian F., Mezzetti M., 1998, *ApJ*, 506, 45
 Hoekstra H., 2003, *MNRAS*, 339, 1155
 Hoekstra H., Yee H. K. C., Gladders M. A., 2004, *ApJ*, 606, 67
 Hobson M. P., Jones A. W., Lasenby A. N., 1999, *MNRAS*, 309, 125
 Hopkins P. F., Bahcall N. & Bode P., 2005, *ApJ*, 618, 1
 Jeltema T. E., Canizares C. R., Bautz M. W., Buote D. A., 2005, *ApJ*, 624, 606
 Jing Y. P., Mo H. J., Börner G., Fang L. Z., 1995, *MNRAS*, 276,

417
 Jing Y. P., Suto Y., 2002, *ApJ*, 574, 538
 Kang X., Mao S., Gao L., Jing Y. P., 2005, *A&A*, 437, 383
 Kazantzidis S., Kravtsov A. V., Zentner A. R., Allgood B., Nagai D., Moore B., 2004, *ApJ*, 611, L73
 Kerscher M., Mecke K., Schmalzing J., Beisbart C., Buchert T., Wagner H., 2001a, *A&A*, 373, 1
 Kerscher M. et al., 2001b, *A&A*, 377, 1
 Kochanek C. S., 2002, in *The Shapes of Galaxies and Their Dark Matter Halos*, ed. Priyamvada Natrajan (World Scientific, Singapore), p. 62, astro-ph/0106495
 Kolb E. W., Turner M. S., 1990, *Early Universe* (Addison-Wesley Publishing Company, USA)
 Kolokotronis V., Basilakos S., Plionis M., Georgantopoulos I., 2001, *MNRAS*, 320, 49
 Libeskind N. I. et al., 2005, *MNRAS*, 363, 146
 Maccio A. V., Moore B., Stadel J., Diemand J., 2005, *MNRAS*, submitted, astro-ph/0506125
 Mecke K. R., Buchert T., Wagner H., 1994, *A&A*, 288, 697
 McMillan S. L. W., Kowalski M. P., Ulmer M. P., 1989, *ApJS*, 70, 723 (MKU)
 Melott A. L., Chambers S. W., Miller C. J., 2001, *ApJ*, 559, L75 (MCM)
 Minkowski H., 1903, *Math. Ann.*, 57, 447
 Motl P. M., Burns J. O., Loken C., Norman M. L., Bryan G., 2004, *ApJ*, 606, 635
 Nagai D., Kravtsov A. V., 2005, *ApJ*, 618, 557
 Narayan R., Medvedev M. V., 2001, *ApJ*, 562, L129
 Natrajan P., Springel V., 2004, *ApJ*, 617, L13
 Norman M. L., Bryan G. L., 1999, *ASSL Vol. 240: Numerical Astrophysics*, eds. S. M. Miyama, K. Tomosaka, T. Hanawa (Kluwer Academic Publishers, Boston), p. 19
 Paz D. J., Lambas D. G., Padilla N., Merchin M., 2005, *MNRAS*,

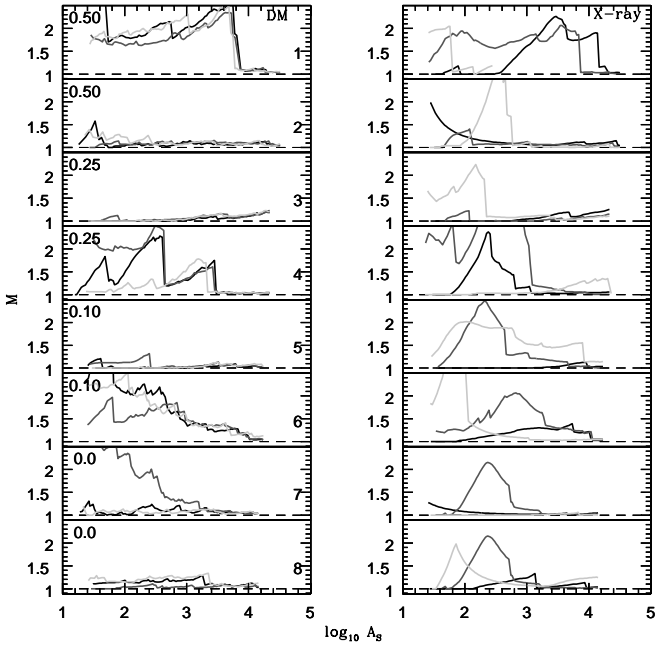


Figure 4. Multiplicity (M) as a function of contour area (A_S) for a selection of clusters at $z = 0.50, 0.25, 0.10,$ and 0.0 . Two clusters from each redshift are shown. Dark, gray, and faint solid lines represent respectively, the adiabatic, radiative cooling (RC), and star formation with feedback (SFF) samples. The dark matter (DM) and X-ray clusters are shown on the left and right panels, respectively. Multiplicity is, in general, greater than 1 in the entire redshift range for clusters simulated with RC (medium line) indicating a slower evolution than in the adiabatic sample (dark line). Redshift $z = 0.5$ is taken for demonstration purpose only. See text for details.

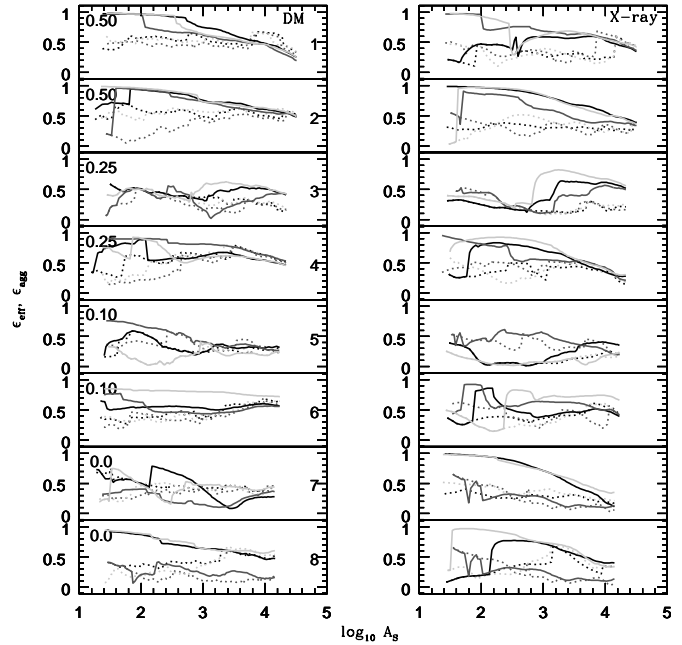


Figure 5. Effective (ϵ_{eff}) and aggregate (ϵ_{agg}) ellipticity as a function of contour area (A_S) for the same clusters as in Fig. 4. Solid and dotted lines are used to represent ϵ_{agg} and ϵ_{eff} , respectively. The color style is similar to Fig. 4. In most cases the non-spherical central part of these clusters consists of a single peak (i.e. $\epsilon_{eff} = \epsilon_{agg}$) whereas in the outer regions sub-clumps show various shapes. It can be seen easily that the central regions of clusters in hydrodynamic simulations appear to be more regular. We notice that cluster centers are slightly more flattened than the outer parts, irrespective of the nature of simulation. Although the trend is weak. See text for details.

submitted, astro-ph/0509062
 Plionis M., 2002, ApJ, 572, L67
 Quinn P. J., Salmon J. K., Zurek W. H., 1986, Nature, 322, 329
 Rhee G. F. R. N., van Haarlem M., Katgert P., 1991, A&AS, 91, 513
 Rahman N., Shandarin S. F., 2003, MNRAS, 343, 933 (RS03)
 Rahman N., Shandarin S. F., 2004, MNRAS, 354, 235 (RS04)
 Rahman N., Shandarin S. F., Motl P. M., Melott A. L., 2004, astro-ph/0405097
 Sarazin C. L., 1988, X-ray emission from clusters of galaxies, Cambridge University Press, Cambridge, New York
 Schmalzing J., 1999, Ph.D. Thesis, Ludwig Maximilians Universität, München, Germany
 Schmalzing J., Buchert T., Melott A. L., Sahni V., Sathyaprakash B. S., Shandarin S. F., ApJ, 526, 568
 Shandarin S. F., Sheth J. V., Sahni V., 2004, MNRAS, 353, 162
 Spergel D. N. et al., 2003, ApJS, 148, 175
 Springel V., White S. D. M., Hernquist L., 2004, in Dark Matter in Galaxies, IAU Symposium, vol. 220, eds. S. D. Ryder, D. J. Pisano, M. A. Walker & K. C. Freeman, p. 421
 Suwa T., Habe A., Yoshikawa K., Okamoto T., 2003, ApJ, 588, 17
 Tissera P. B., Dominguez-Tenreiro R., 1998, MNRAS, 297, 177
 Thomas P. A. et al., 1998, MNRAS, 296, 1061
 Trèvese D., Flin P., Migliori L., Hickson P., Pittella G., 1992, A&ASS, 94, 327
 Trèvese D., Cirimele G., Cenci A., Appodia B., Flin P., Hickson P., 1997, A&ASS, 125, 459

Valdarnini R., Ghizzardi S., Bomometto S., 1999, New Astronomy, 4, 71
 van den Bosch F. c., Yang X., Mo H. J., Norberg P., 2005, MNRAS, 356, 1233
 Voit M. G., Bryan G. L., Balogh M. L., Bower R. G., 2002, ApJ, 576, 601
 Warren M. S., Quinn P. J., Salmon J. K., Zurek W. H., 1992, ApJ, 399, 405
 West M. J., Bothun G. D., 1990, ApJ, 350, 36
 Westbury C. F., Henriksen R. N., 1992, ApJ, 338, 64
 Zentner A. R., Berlind A. A., Bullock J. S., Kravtsov A. V., Wechsler R. H., 2005, ApJ, 624, 505

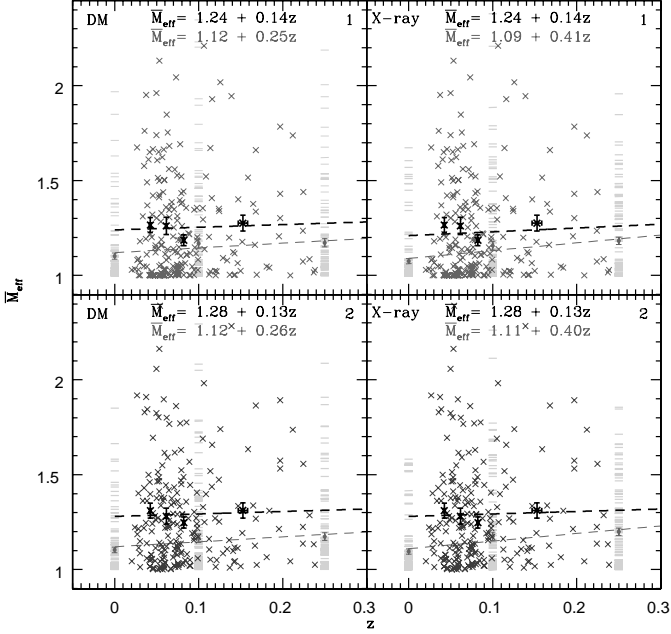


Figure 6. A detailed comparison of the estimate of \bar{M}_{eff} for the adiabatic DM (left panels) and X-ray (right panels) clusters and the optical sample with $ss=50 h^{-1} \text{ kpc}$ within $0.5 h^{-1} \text{ Mpc}$ (panels 1) and $1.0 h^{-1} \text{ Mpc}$ (panels 2) radius. Simulated clusters are shown by (faint) horizontal lines at $z = 0.25, 0.10, 0.0$ and the optical clusters are shown by (dark) crosses. The expressions represent the best fit lines for observation (dark; top line in each panel) and simulation (faint; second line in each panel).

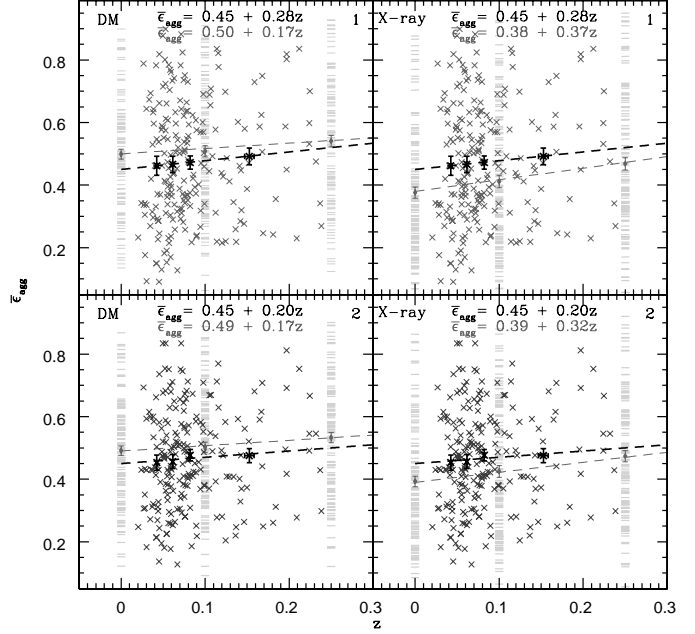


Figure 7. A detailed comparison of the estimate of $\bar{\epsilon}_{agg}$ obtained from the adiabatic DM (left panels) and X-ray (right panels) clusters and from the optical sample. Presentation style is similar to Figure 6.

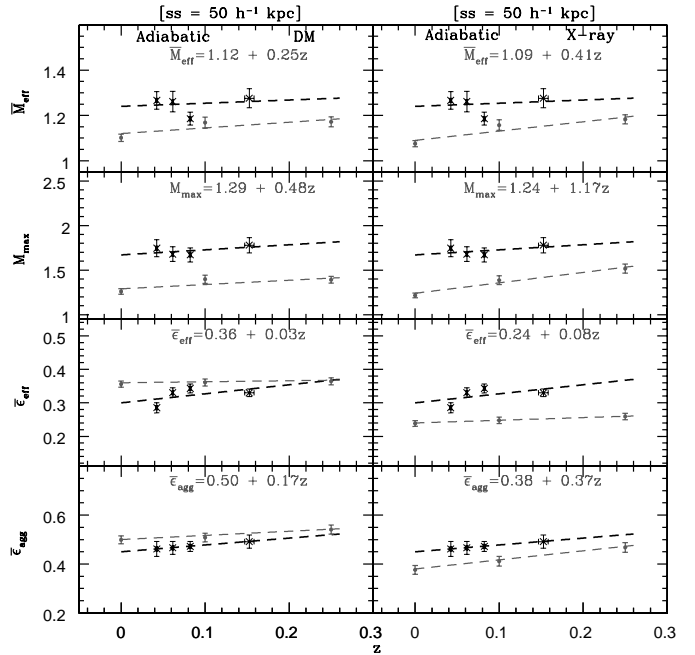


Figure 8. Adiabatic sample with $50 h^{-1} \text{ kpc}$ smoothing (ss) within $0.5 h^{-1} \text{ Mpc}$ radius. Dark and gray lines are used for optical and simulated clusters, respectively. The error bar represents the error in the mean. The expression at each panel relate the evolution of the mean value of the parameter of with redshift. The strength of evolution for optical clusters are: $d\bar{M}_{eff}/dz \sim 0.14$, $dM_{max}/dz \sim 0.57$, $d\bar{\epsilon}_{eff}/dz \sim 0.27$, and $d\bar{\epsilon}_{agg}/dz \sim 0.28$.

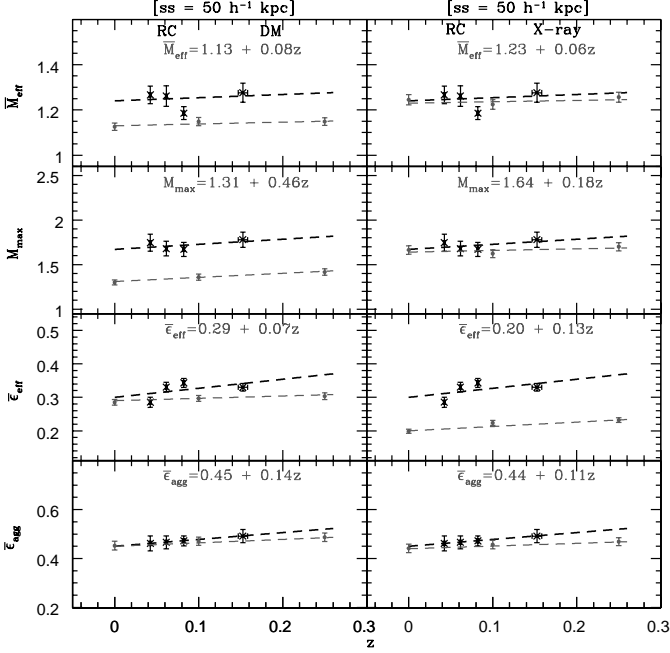


Figure 9. Radiative cooling (RC) sample with $50 \text{ h}^{-1} \text{ kpc}$ smoothing (ss) within $0.5 \text{ h}^{-1} \text{ Mpc}$ radius. Presentation style is similar to Fig. 8.

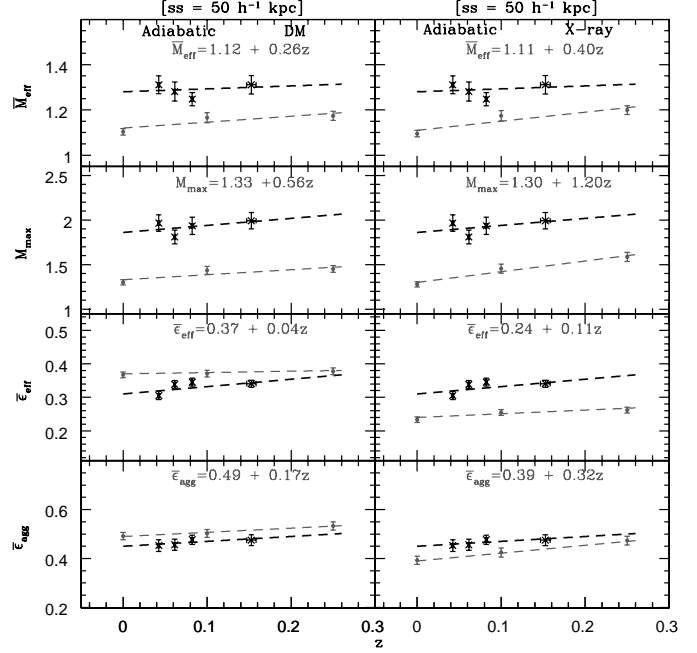


Figure 11. Adiabatic sample with $50 \text{ h}^{-1} \text{ kpc}$ smoothing (ss) within $1.0 \text{ h}^{-1} \text{ Mpc}$ radius. Presentation style is similar to Fig. 8. The strength of evolution for optical clusters are: $d\bar{M}_{eff}/dz \sim 0.13$, $dM_{max}/dz \sim 0.79$, $d\bar{\epsilon}_{eff}/dz \sim 0.22$, and $d\bar{\epsilon}_{agg}/dz \sim 0.20$.

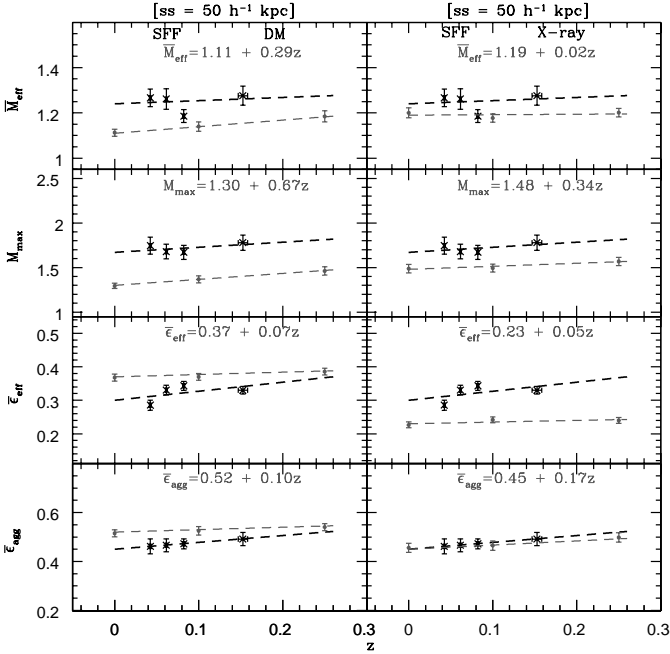


Figure 10. Star formation with feedback (SFF) sample with $50 \text{ h}^{-1} \text{ kpc}$ smoothing (ss) at $0.5 \text{ h}^{-1} \text{ Mpc}$ radius. Presentation style is similar to Fig. 8.

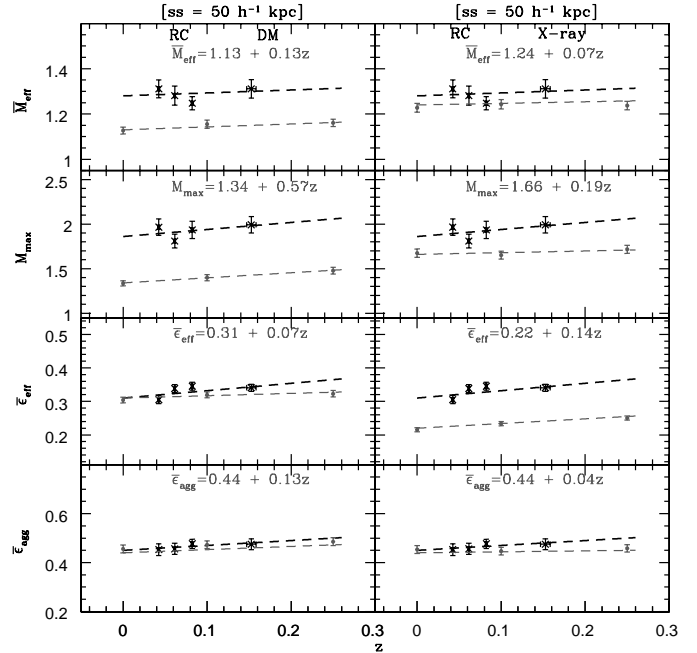


Figure 12. Radiative cooling (RC) sample with $50 \text{ h}^{-1} \text{ kpc}$ smoothing (ss) within $1.0 \text{ h}^{-1} \text{ Mpc}$ radius. Presentation style is similar to Fig. 8.

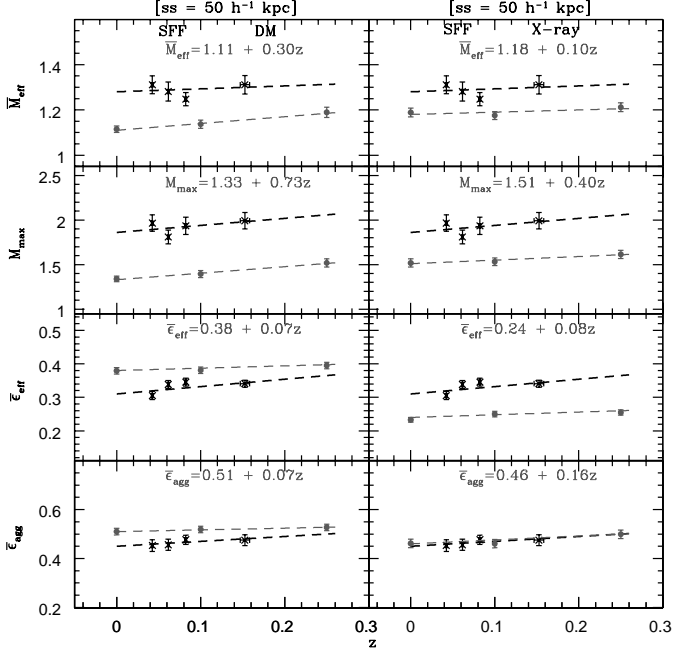


Figure 13. Star formation with feedback (SFF) sample with $50 \text{ h}^{-1} \text{ kpc}$ smoothing (ss) within $1.0 \text{ h}^{-1} \text{ Mpc}$ radius. Presentation style is similar to Fig. 8.